

## RESEARCH ARTICLE

Polymer  
COMPOSITES

WILEY

# Effect of ceramic nano-particles on the properties of a carbon-phenolic ablator

Laura Paglia<sup>1</sup> | Caterina Mapelli<sup>2</sup> | Virgilio Genova<sup>1</sup> |  
 Maria Paola Bracciale<sup>1</sup> | Francesco Marra<sup>1</sup> | Cecilia Bartuli<sup>1</sup> |  
 Ilaria Fratoddi<sup>3</sup> | Giovanni Pulci<sup>1</sup>

<sup>1</sup>Department of Chemical Engineering Materials Environment, INSTM Reference Laboratory for Engineering of Surface Treatments, Sapienza University of Rome, Rome, Italy

<sup>2</sup>Department of Chemistry, University of York, York, UK

<sup>3</sup>Department of Chemistry, Sapienza University of Rome, Rome, Italy

## Correspondence

Laura Paglia, Department of Chemical Engineering Materials Environment, INSTM Reference Laboratory for Engineering of Surface Treatments, Sapienza University of Rome, Rome, Italy. Email: [laura.paglia@uniroma1.it](mailto:laura.paglia@uniroma1.it)

## Funding information

Università degli Studi di Roma La Sapienza

## Abstract

Carbon-phenolic ablaters are very efficient heat shields for atmospheric reentry vehicles: they are able to protect a capsule from hyper thermal environments characterized by intense heat fluxes ( $>1 \text{ MW/m}^2$ ) and very high temperature (also exceeding  $300^\circ\text{C}$ ). Ablative materials can be modified by the addition of nano-fillers in order to improve their performance: small amounts of nano-fillers (in the order of 2–5 wt%) are able to enhance the matrix material properties, guarantying a weight saving too. In this work, three different kinds of ceramic nano-particles ( $\text{ZrO}_2$ , SiC, and MgO) were tested as fillers for a phenolic resin and for a carbon-phenolic ablator: the variation in the mechanical properties and ablative performances were verified through mechanical tests and oxyacetylene flame exposure. The influence of the nano-particles in the composite materials properties and the phenomena connected to their presence in the ablative material were deeply investigated with scanning electron microscope, EDS, XRD, and FTIR analysis.

## KEYWORDS

carbon-phenolic ablative materials, FTIR analysis, mechanical tests, nano-composites

## 1 | INTRODUCTION

Nano-composite materials have found great consents since their first applications in early 90s because of the possibility to improve or change the properties of a matrix by the addition of small quantities of nano-fillers.<sup>[1–5]</sup> Nano-composites can be manufactured with different kinds of matrices (ceramic, metal, and polymer) and with different nano-fillers which distinguish not only for their composition but also for their shape and aspect ratio (e.g., nanoparticles, nanowires, and nanoplatelets).<sup>[1,6,7]</sup>

According to the kind of matrix (ceramic, metal or polymer) the toughening and strengthening mechanisms of the nano-fillers can be very different: for example, for ceramic or metallic matrix, nano-fillers are able to modify the microstructure during the manufacturing process of sintering, changing the shape and the size of the crystal grains<sup>[5]</sup>; in a polymer the nano-fillers can create an interphase zone between reinforcement and matrix with unique thermo-mechanical and thermo-physical properties able to deeply modify the composite behavior.<sup>[2,8]</sup> This interphase zone is present both in conventional and

This is an open access article under the terms of the [Creative Commons Attribution-NonCommercial-NoDerivs](https://creativecommons.org/licenses/by-nc-nd/4.0/) License, which permits use and distribution in any medium, provided the original work is properly cited, the use is non-commercial and no modifications or adaptations are made.

© 2022 The Authors. *Polymer Composites* published by Wiley Periodicals LLC on behalf of Society of Plastics Engineers.

nano-composites but, for the last ones, the interfacial area per unit volume ( $R$ ,  $\text{m}^2/\text{cm}^3$ ) becomes ultra-large because of the huge surface/volume ratio of nano-fillers and its influence on the overall properties of the materials is more relevant.<sup>[7,8]</sup>

Since small amounts of nano-fillers are able to modify the properties of a bulk material, the final density of the nano-composite does not differ significantly from the bulk material's one. For this reason, this reinforcement strategy can be very interesting for materials adopted in the heat shields of the atmospheric reentry vehicle, where the weight saving is a critical issue.<sup>[9]</sup> Vehicles going through an interplanetary atmosphere suffer intense heating because of the friction between the surfaces of the vehicle and the atmospheric gasses.<sup>[6,8]</sup> When heat fluxes exceed  $1 \text{ MW}/\text{m}^2$ , for example for ballistic atmospheric reentry, ablative carbon-phenolic heat shields are typically selected: these materials consist of reinforcing carbon fibers fully or partially infiltrated by a phenolic resin and they are semi-active insulators, able to protect the inner part of the vehicle because of their insulating properties and because of the endothermic reactions related to the polymer matrix decomposition. The produced pyrolysis gasses, flowing through the char and into the boundary layer, are able both to absorb part of the incoming heat and to hinder the convective exchanges (this is the so called blockage effect).<sup>[8,10–12]</sup>

During the last 20 years, several studies were carried out with the attempt of modifying ablative composite materials with the addition of nano-fillers. Srikanth et al.<sup>[13]</sup> modified a high density carbon-phenolic ablator with nanoparticles of  $\text{SiO}_2$  and tested the blank and the modified materials under a plasma arc jet at  $2.5 \text{ MW}/\text{m}^2$ . Nano-composite ablators with an amount of 2% wt of nano- $\text{SiO}_2$  showed a better performance in terms of ablation rate. Robert et al.<sup>[14]</sup> studied the behavior of nano-composite ablators based on phenolic resin reinforced with chopped silica fiber and nano-clay: results showed that the proper amount of nano-fillers guarantees enhanced mechanical and ablative properties. Parks et al.<sup>[15]</sup> proved beneficial effect in the ablative performance of phenolic resin composites when reinforced with Multi-Wall Carbon Nano-Tubes (MWCNT). The success of the reinforcing phase always depends on the amount, distribution and dispersion of the nano-particles inside the matrix.<sup>[13–17]</sup>

In this work  $\text{ZrO}_2$ ,  $\text{SiC}$ , and  $\text{MgO}$  nano-particles were selected to be added to a lightweight carbon-phenolic ablator ( $\rho \sim 0.3 \text{ g}/\text{cm}^3$ ) for their low density, low thermal conductivity, and high melting point. At first, samples of phenolic resin and nano-particles were manufactured in order to understand the influence of the nano-fillers on the mechanical properties of the unreinforced phenolic resin. Then, the same nano-particles were used to

manufacture nano-composite ablators, which were tested at a heat flux of  $4 \text{ MW}/\text{m}^2$  by an oxyacetylene torch. Compression tests on charred samples of standard and nano-composite materials were carried out to understand the effect of nano-particles addition on the mechanical performance of the char. Nano-particles influenced not only the performances of the ablative materials, but also the manufacturing process: for example the presence of nano- $\text{MgO}$  accelerates the curing time. This phenomenon was investigated with FTIR analysis in order to fully understand the interaction mechanisms: understanding the molecular structure of the resin and the chemical mechanism involved in the cure process is crucial not only to improve the manufacturing process but also to optimize the performance of the ablative material. In fact, the cross-linking density of the phenolic resin has been associated with the char-yield,<sup>[18]</sup> that is an important property influencing the ablation process. This work proposes also a deep analysis, of the nano-particles after the oxyacetylene burner exposure of the ablative materials through SEM, EDS, and XRD analysis. The aim of this characterization is to understand if all phenomena connected to nano-particles can be considered beneficial or not for the performance of the ablator.

## 2 | EXPERIMENTAL

### 2.1 | Raw materials

Phenolic resin Durite SC-1008, provided by Hexion, is selected as matrix for the proposed nano-composite materials. It is a commercial phenolic resin characterized by a good char yield and its properties, according to the supplier data sheet, were reported elsewhere.<sup>[19]</sup>

The reinforcing phase consists of a commercial carbon felt, MFA Sigratherm (SGL Carbon) which is provided in tiles of  $10 \times 10 \times 4 \text{ cm}^3$ . The carbon fibers have an average diameter of  $10 \mu\text{m}$  and the section have the peculiar shape shown in Figure 1. The felt tiles consist of nonwoven fibers randomly distributed into the plane, thus leading to isotropic in-plane properties. Two different solvents were used to dilute the phenolic resin: ethylene glycol (boiling point of  $197^\circ\text{C}$ ), and 1-propanol (boiling point of  $97^\circ\text{C}$ ). The ethylene glycol was selected for the manufacturing of the ablative samples because it promotes the formation of a gel phase during the curing process of the phenolic resin. The gel phase is beneficial for a homogeneous distribution of the resin within the carbon felt and it could hinder the agglomeration of the nano-particles.<sup>[8]</sup> 1-Propanol is used for the manufacturing of nano-filled phenolic samples, without carbon felt. These samples were produced to be mechanically tested by four points bending test with the

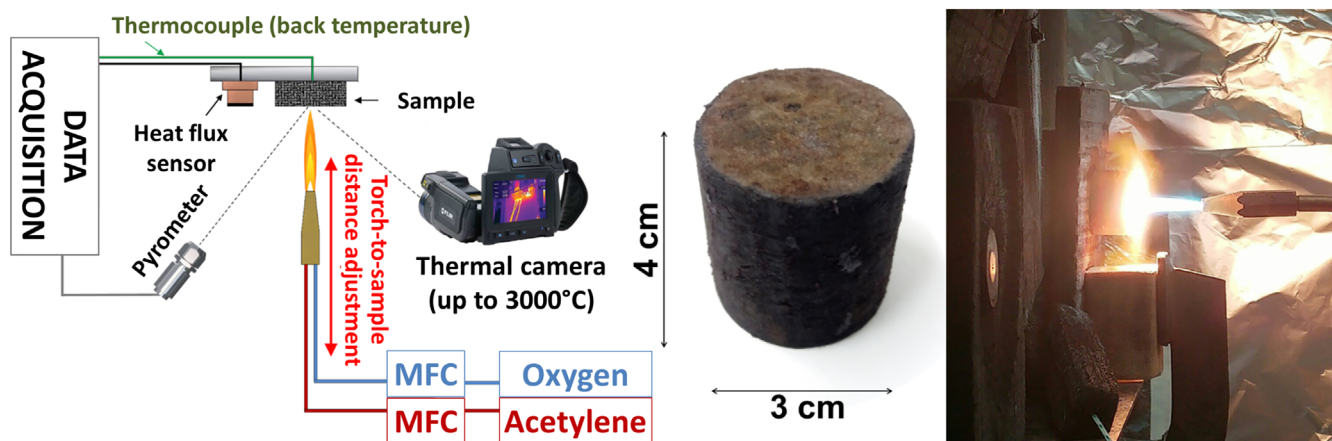


**FIGURE 1** Scheme of the oxyacetylene flame burner facility (left), a sample before testing (center) and an for peer review ongoing oxyacetylene flame exposure test (left)

**TABLE 1** Ceramic nano-particles properties according to technical data sheet (IoLiTec GmbH)

	Average particle size (nm)	Density (g/cm <sup>3</sup> )	Melting temperature (°C)
ZrO <sub>2</sub>	50	5.7	2715
SiC	40	3.2	2700
MgO	30	3.6	2850

aim of understanding the mechanical effect of the nano-particles on the phenolic resin. Ceramic nano-fillers were selected for this experimentation because of their thermal and mechanical properties: the addition of ceramic particles could improve the mechanical strength of the carbonaceous residue and enhance the insulation properties of the ablative material.<sup>[6]</sup> Previous works<sup>[8,10,11]</sup> highlighted a significant properties improvement in nano-filled ablators exposed to high heat fluxes: in this work ZrO<sub>2</sub>, SiC, and MgO ceramic nano-particles were selected to modify the standard carbon-phenolic ablator. Zirconium oxide nanofillers were selected because of the high melting temperature and low thermal conductivity<sup>[8,11]</sup>; SiC, successfully proved as reinforcing phase in previous works, was chosen because of the ability to improve the thermo-mechanical properties of phenolic-based composites.<sup>[20,21]</sup> MgO was chosen as a new candidate for reinforcing this kind of material because of its low density and high melting point. Nanoparticles were provided by IoLiTec GmbH (Germany) and their main properties are reassumed in Table 1.

## 2.2 | Manufacturing procedure

Bulk samples of plain and nano-filled phenolic resin were manufactured to be mechanically tested. The goal of this

**TABLE 2** Cure in oven for samples of bulk resin

Step	Duration (h)	Temperature (°C)
1	24	85
2	24	98
3	24	113
4	72	127
5	24	138

manufacturing step was to produce uniform and compact samples, without porosity and cracks; the nano-particles were at first add to the 1-propanol and sonicated in a ultrasonic bath (Elmasonic S30H), then the suspension was mixed to the phenolic resin. The solution was poured into a silicone mold and further sonicated in an ultrasonic bath for 7 h at 60°C. This procedure allows for evacuating the low boiling point solvent and increasing the viscosity of the phenolic resin hindering the agglomeration of nano-particles. Then the samples were cured in oven to remove the residual solvent and to allow for the complete polymerization. This cure step has to be very slow in order to avoid defects within the samples. The curing procedure is reassumed in Table 2. The manufacturing process is the same for all nano-composite samples and it was optimized for avoiding formation of defects and to guarantee a good dispersion of the nano-

particles. The cured bulk resin and nano-filled resins were machined and polished to obtain four points bending test samples according to the ASTM standard D790-00.<sup>[22]</sup>

The carbon-phenolic ablators modified by ceramic nanoparticles were produced with a final density of about 0.3 g/cm<sup>3</sup> following a procedure optimized in a previous work.<sup>[8]</sup> Cylindrical samples of carbon felt (Sigratherm MFA—3 cm in diameter, 3 cm in height) were infiltrated with a solution of phenolic resin and ethylene glycol enriched with ZrO<sub>2</sub>, SiC or MgO nano-particles. The gelation process occurring in the resin/ethylene glycol solution during the first step of polymerization can promote the immobilization of the dispersed nano-particles and the formation of an homogeneous porous polymeric structure within the carbon felt. At first the nano-particles were added to the solvent and dispersed by a high power sonication probe (Fisher Scientific, Model 505 Sonic Dismembrator) (step 1), then the resin was added and the sonication was repeated (step 2). After the sonication steps, the solution was heated and stirred on a hot plate: the heat promotes the evacuation of the solvent and the stirring contributes to keep a homogeneous temperature and partially hinders the agglomeration of the nano-particles (step 3). The duration of this step depends on the presence and type of nano-particles added to the

solution: for all the different compositions the heating was interrupted at the early stage of gel formation. After this heating phase, the solution was cooled down to a temperature of 80°C in order to carry out a further sonication process aimed at eliminating agglomerates and reducing the viscosity in order to facilitate the infiltration of the carbon felt preforms (step 4). The cylinder-shaped felts were submerged inside the solution, covered and put inside a muffle furnace to promote the complete process of gelation (step 5). Then, the samples were removed from the gel and put again in the furnace for the final cure in order to obtain the complete polymerization of the phenolic resin (step 6). Each manufacturing step is characterized by a specific duration and temperature, as reassumed in Table 3.

All the samples (carbon-phenolic ablators and resin samples without felt) were manufactured with the same amount of nano-particles in terms of weight percentage (5% wt) with respect to the final weight of resin. The composition and the nomenclature for all manufactured samples are reassumed in Table 4.

**TABLE 3** Duration and temperature for each step of the manufacturing procedure

Step	Duration	Temperature
1	2 h	RT
2	1 h	RT
3	150 min (no nano-particles) 180 min (with ZrO <sub>2</sub> ) 180 min (with SiC) 90 min (with MgO)	156°C
4	1 h	<80°C
5	15 h	180°C
6	24 h	180°C

### 2.3 | Mechanical characterization

Four points bending tests were carried out on bulk resin samples according to the ASTM standard D 790-00<sup>[22]</sup> with a Zwick Roell mechanical testing machine Z010 equipped with a 10 kN load cell. A distance of 5 cm was selected for the lower supports while the upper supports span was 2.5 cm. The tests were carried out on parallelepiped-shaped specimen (80 mm × 25 mm × 5 mm) with a crosshead rate of 2 mm/min and the samples strain was measured by a contact extensometer. Five samples were tested for each kind of material: bulk phenolic resin (P0) and nano-charged resins (PZ, PS, PM).

Compression tests on pyrolyzed nano-composite ablators were performed according to the ASTM C165-07.<sup>[23]</sup> Three cylindrical specimens for each kind of ablator were charred in a high temperature tube furnace (Carbolite Gero,

Name	Carbon felt	Phenolic resin	Solvent	Nano-particles
P0	–	Durite SC 1008	1-Propanol	–
PZ	–	Durite SC 1008	1-Propanol	ZrO <sub>2</sub> (50–100 nm)
PM	–	Durite SC 1008	1-Propanol	MgO (35 nm)
PS	–	Durite SC 1008	1-Propanol	SiC (50–60 nm)
MP0	MFA Sigratherm	Durite SC 1008	Ethylene glycol	–
MPZ	MFA Sigratherm	Durite SC 1008	Ethylene glycol	ZrO <sub>2</sub> (50–100 nm)
MPM	MFA Sigratherm	Durite SC 1008	Ethylene glycol	MgO (35 nm)
MPS	MFA Sigratherm	Durite SC 1008	Ethylene glycol	SiC (50–60 nm)

**TABLE 4** Manufactured samples: nomenclature and composition

TF1-1600) equipped with a dense alumina tube. The samples were heated in inert atmosphere (Ar, 2 N L/min) from RT to 900°C with a heating rate of 5°C/min, then the temperature of 900°C was kept for 1 h followed by a cooling phase with a rate of 5°C/min. This procedure guarantees the complete polymerization of the samples according to the thermogravimetric analysis (Sections 2.4–3.4). All samples were weighted before and after the pyrolysis in order to verify the charring. As for the bending tests, the compression tests were carried out with Zwick Roell mechanical testing machine Z010 equipped with a 10 kN load cell with a testing speed of 10 mm/min.

## 2.4 | Thermogravimetric analysis

Thermogravimetric analyses were carried out on samples of phenolic resin modified by nano-particles at an heating rate of 10°C/min with a TG analyzer (Q600, TA Instrument) in argon atmosphere. In order to guarantee constant atmospheric conditions, the pyrolysis gas, produced during the heating, is removed by a continuous flux of argon at 100 ml/min. The temperature during the test varies from RT to 1000°C. All samples were previously reduced to powder and divided with the quartering method for obtaining the desired mass of about 10 mg for each test.

## 2.5 | Spectroscopical characterization

Fourier transform infrared (FT-IR) spectra of phenolic resin and nano-filled phenolic resin were acquired using a Bruker Vertex 70 in the 4000–400 cm<sup>-1</sup> range. After the cure process, samples were grinded into a fine powder using an agate mortar and dispersed into CHCl<sub>3</sub> (Sigma Aldrich). The dispersion was then deposited as thin film on the thallium bromoiodide (KRS-5) window allowing the solvent to evaporate.

## 2.6 | Oxyacetylene flame exposure

Oxyacetylene flame burner exposure tests were carried out on carbon-phenolic ablators according to the ASTM standard E 285–08.<sup>[24]</sup> This characterization test is specifically designed to determine the relative thermal insulation effectiveness of the different ablators.<sup>[25]</sup> The facility used for performing this test was designed and engineered by the Laboratory of Materials and Surface Engineering of Sapienza University of Rome. The same facility was used for previous works<sup>[8,10,11,26]</sup> but it was gradually improved to obtain more and more accurate

results. Figure 1 shows a scheme of the facility: the oxyacetylene flame is the result of the combustion of oxygen and acetylene carried to the burner through two supply lines. According to the proportion of fuel and oxidizer it is possible to obtain an oxidizing, a neutral or a reducing flame. For this kind of test it is important to have a neutral or a reducing flame in order to activate the pyrolysis reactions and avoid the catastrophic oxidation of the ablators. The facility is equipped with a heat flux sensor (HFM 1000 Vatell Corporation, Christiansburg, VA) for calibrating and measuring the cold wall heat flux; a two-color digital pyrometer (Impac Infrared, Frankfurt, Germany) for recording surface temperatures; a k-thermocouple for recording temperature inside or at the back of the specimen and an infrared thermal camera calibrated up to 3000°C (Flir A655sc). A data acquisition system (National Instrument) acquires and records the data during the test while LabView software provides a virtual interface for managing input and output parameters. The gas pressure and flow rate were set at 1.15 bar–315 NL/h (acetylene) and 3.5 bar–300 NL/h (oxygen). The specimens were exposed to a heat flux of 4 MW/m<sup>2</sup> for a time of 90 s. A test sample and an ongoing test picture are shown in Figure 1.

## 2.7 | X-ray diffraction analysis

XRD analyses were carried out both for the as-received MgO nano-particles and for the nano-particles after the oxyacetylene flame exposure. The XRD spectra were obtained with a Philips X'Pert X-ray device (PANalytical B.V., The Netherlands) operating at 40 kV and 40 mA with CKuα1 radiation. The scan range selected for the samples was of 20°–80°, step size of 0.02° and counting time of 2 s.

# 3 | DISCUSSIONS AND RESULTS

## 3.1 | Microstructural characterization

Nano-composite phenolic resin samples and nano-composites ablators were cut, polished and prepared to be observed with a Scanning Electron Microscope (Tescan Mira3). The analysis of the microstructure of the nano-filled samples is mandatory to assess whether the manufacturing processes are appropriate for obtaining this peculiar kind of materials.

Micrographs of the nano-charged resin samples are shown in Figure 2: in PZ sample (image [A]) the nano-ZrO<sub>2</sub> distribution is quite satisfying because nano-particles are homogeneously distributed and there are

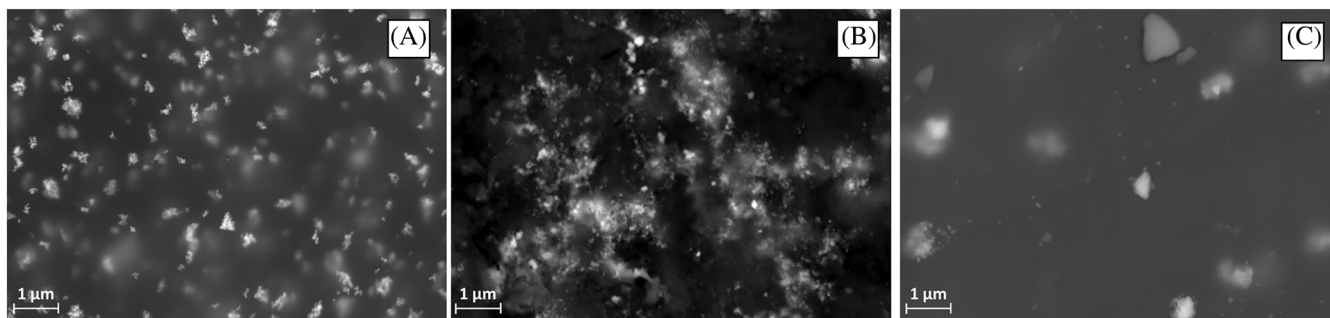


FIGURE 2 SEM images of nano-composites: (A)  $ZrO_2$ , (B) SiC, and (C) MgO inside the phenolic resin (samples of PZ, PS, PM)

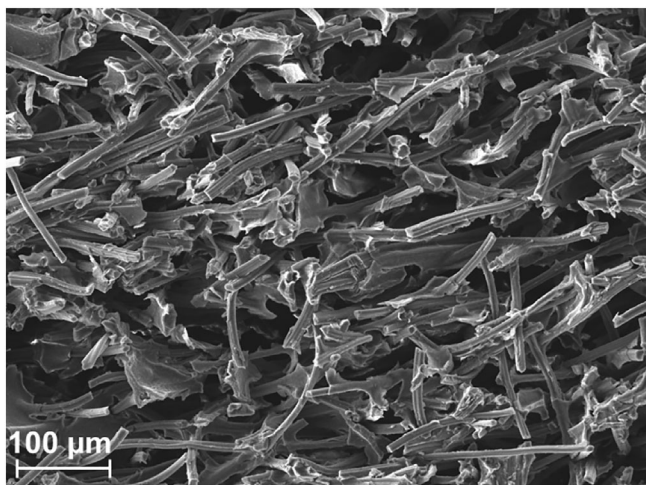


FIGURE 3 Secondary electrons micrograph of a carbon phenolic ablator (MP0)

agglomerates not larger than 300 nm. The micrograph (B) in Figure 2 is referred to the nano-SiC modified phenolic resin and it enlightens the inadequate distribution of the nano-particles that are present in form of large agglomerates. MgO nano-particles (image [C]) are distributed in the whole PM samples and, even if single particles can be found dispersed inside the resin, there are also micrometric agglomerates potentially deleterious for the efficiency of the reinforcing mechanisms typical of the nano-composites.<sup>[7,21]</sup> It is important to underline that  $ZrO_2$ , MgO, and SiC nano-particles are added in equal mass fraction with respect to the final mass of resin and, considering their different density (Table 1), there is a consequent difference in the volumetric content. In particular, the reinforcement fraction of  $ZrO_2$  is lower in volume, thus facilitating the distribution of the nano-reinforcement.

For the carbon-phenolic ablative materials the phenolic resin is required to be homogeneously distributed among the fibers and the nano-particles have to be well dispersed and distributed within the cured resin. The micrograph in Figure 3 shows the microstructure of a

MP0 sample (carbon-phenolic without nano-particles) obtained with the optimized manufacturing process described in Section 2.2: the phenolic resin is well distributed in form of thin flakes among the fibers and partially coats the carbon fibers. All nano-filled materials show a comparable microstructures and a homogeneous distribution of the phenolic resin. Anyway at higher magnification (Figure 4) several differences in the morphology of the cured resin can be highlighted: the surface appears to be rougher for samples enriched with SiC nano-particles and smoother for samples modified by nano-MgO; no appreciable differences can be enlighten between MP0 and nano- $ZrO_2$ -modified samples.

In addition, the nano-modified carbon-phenolic samples were observed for verifying the quality of nano-particles distribution. The micrographs in Figure 5A prove the good dispersion and distribution of the nano- $ZrO_2$ : some agglomerations are well visible, but higher magnifications show a satisfying dispersion. The EDS spectrum confirms the nature of the particles. In Figure 5B,C the presence of the SiC and MgO nano-particles is verified by Back Scattered Electrons (BSE) micrographs and EDS spectra: in both cases a good distribution is observed even if some agglomerates can be identified. SEM and EDS analyses prove the goodness of the manufacturing process: the microstructure of the different samples is homogenous and there is only a slight difference in the cured resin roughness, furthermore the nano-particles were incorporated in the final samples with a good dispersion and distribution.

### 3.2 | Mechanical tests results

Four points bending tests were carried out on five specimens for nano-charged and unreinforced phenolic resin (P0, PZ, PS, PM). All the samples exhibit a brittle fracture, as shown in Figure 6. The rupture of samples P0 always causes the formation of two coherent fracture surfaces, while all the nano-composite samples exhibit a

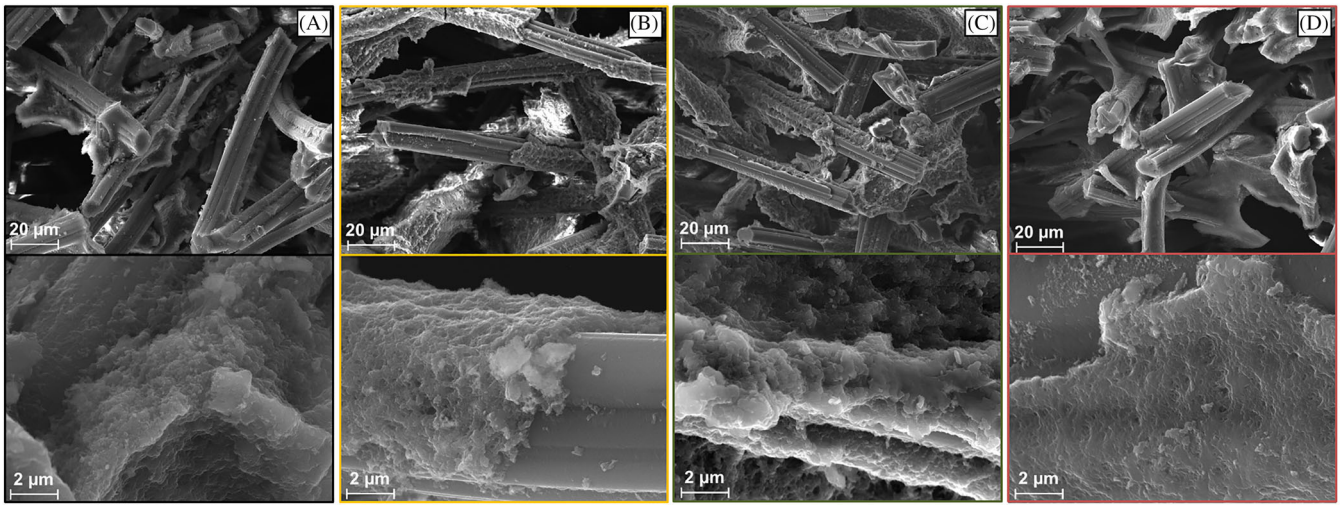


FIGURE 4 SE micrographs of nano-charged ablators: (A) MP0, (B) MPZ, (C) MPS, and (D) MPM

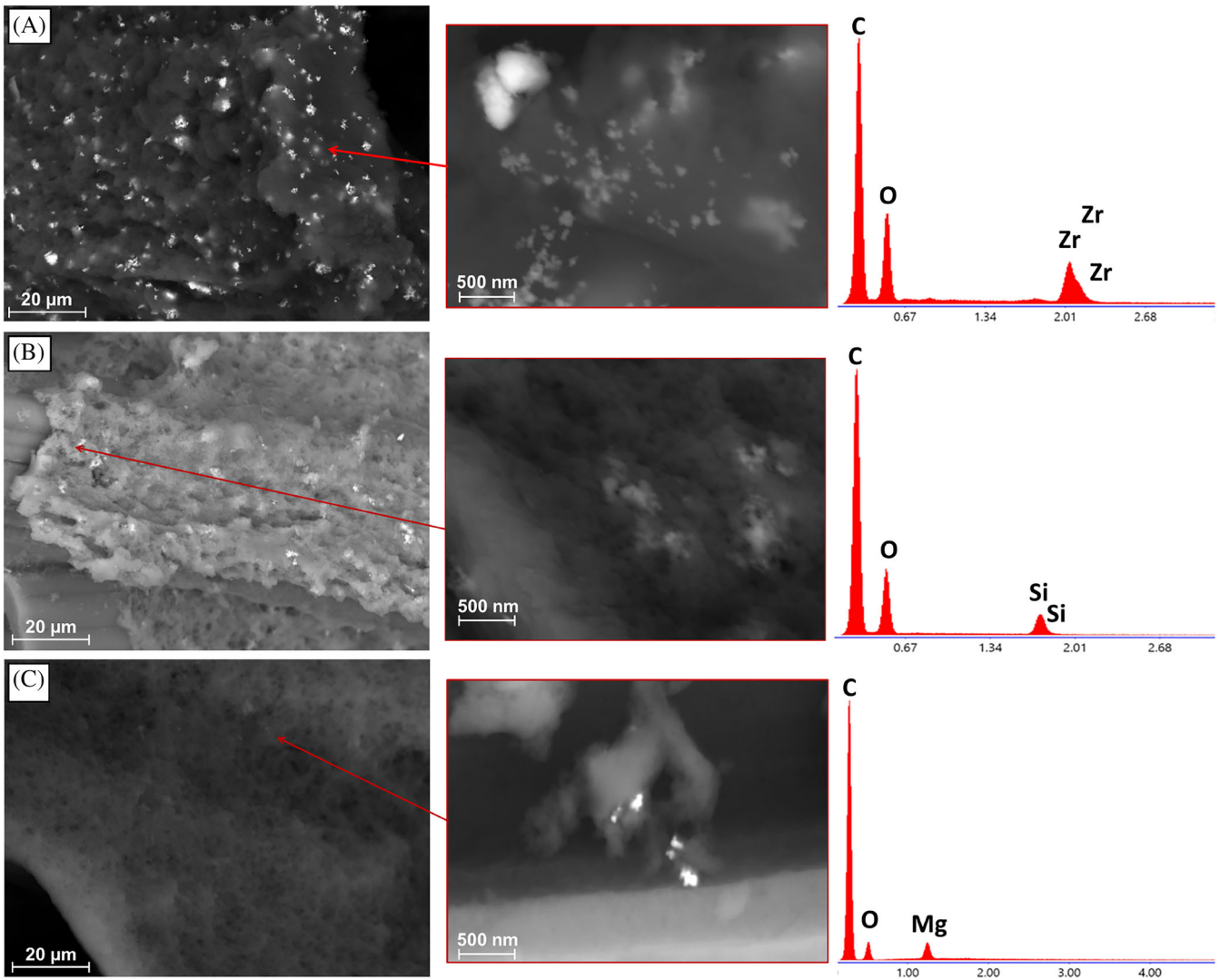


FIGURE 5 BSE micrographs and EDS analysis for MPZ (a), MPS (B), and MPM (C) samples

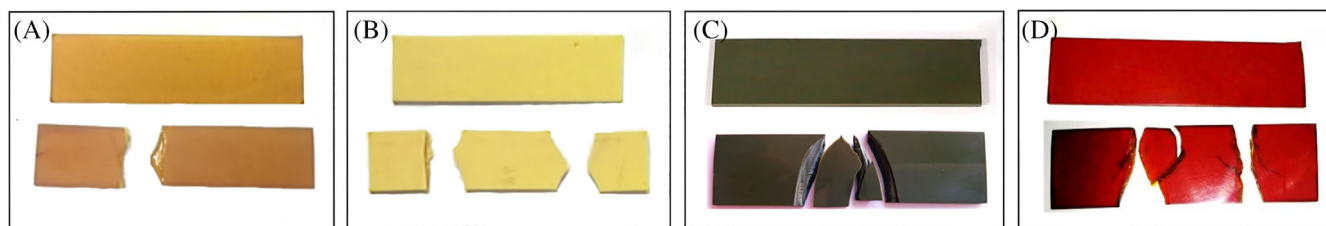


FIGURE 6 Phenolic resin samples before and after the mechanical test ((A) P0; (B) PZ; (C) PS; (D) PM)

TABLE 5 Results of mechanical test on P0, PZ, PS, PM samples

Sample	$E$ (GPa)	$\sigma_{\max}$ (MPa)
P0	$4.7 \pm 0.2$	$137 \pm 9$
PZ	$5.2 \pm 0.1$	$186 \pm 5$
PS	$4.8 \pm 0.7$	$116 \pm 35$
PM	$5.2 \pm 0.6$	$146 \pm 13$

fragmentation mechanism at the failure, as shown in the pictures. In Table 5 the results of the bending tests were reassumed: the Young modulus for samples PZ, PS, and PM is comparable or higher compared with the P0 samples. The improvement is important for samples PZ and PM ( $\sim +11\%$ ), while the Young modulus is unchanged for PS samples. The analysis of flexural strength results highlights the increase induced by  $ZrO_2$  nano-particles addition ( $+35\%$ ) while SiC-modified samples (PS) show a decrease in performance ( $\sim -15\%$ ) and a large dispersion of data ( $\sim 30\%$  of standard deviation).

P0 and PZ exhibit on the contrary a lower standard deviation compared to PS and PM for both Young's modulus and flexural strength data: these results can be attributed to the worse SiC and MgO nano-particles distribution and to the presence of internal defects in the PS and PM resin samples, thus leading to a higher dispersion of the test data. The phenomenon is more emphasized for the samples charged with nano-particles of SiC: these results are in line with the observation of the samples microstructure discussed in Section 3.1. These results show that nano-particles, in the selected percentage, can improve the mechanical properties of the phenolic resin as long as a good dispersion and distribution of nano-particles within the polymer is guaranteed.

Compression stress to strain curves of pyrolyzed ablators are shown in the graph of Figure 7. For each kind of ablator only the most representative curve was selected. It is possible to observe that addition of nano-particles is always beneficial for improving the mechanical performance of the material. The compression curves always follow the same trend: there is a first almost linear section of the curve, then the deformation significantly increases for a slight increase in the compressive stress

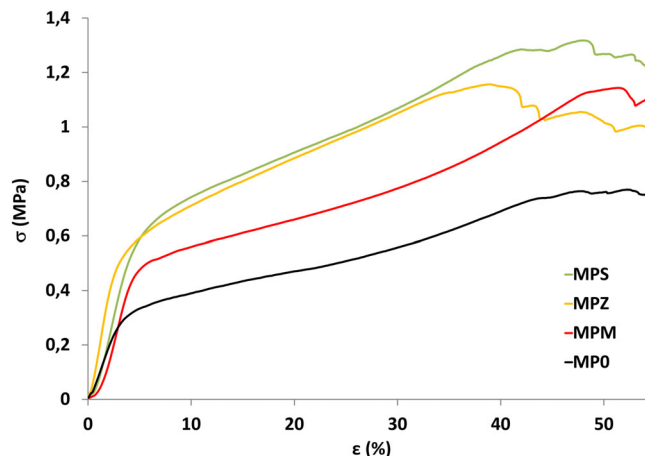


FIGURE 7 Representative  $\sigma$ - $\epsilon$  compression curves for standard and nano-composite ablators

and, finally, an irregular trend is symptomatic of the imminent rupture of the sample.

Results of the maximum stress reached by the samples and the compressive modulus of elasticity (considering the slope of the first straight section of each curve<sup>[23]</sup>) are reassumed in Table 6. SiC and  $ZrO_2$  addition can increase the initial stiffness of the material more than the MgO, while the maximum stress before the imminent rupture is comparable for the three nano-composites ablators and higher of about 70% than the standard ablator.

All the experimental results show that enrichment of phenolic resin or carbon/phenolic ablators with nano-particles is always beneficial in terms of mechanical properties, but the effect is more important for charred ablators. This can be due to the different manufacturing procedure, which, in the case of ablative materials, facilitates the good distribution of the nano-particles as shown in the previous micrographs (Figures 2 and 5).

### 3.3 | Thermogravimetric analysis results

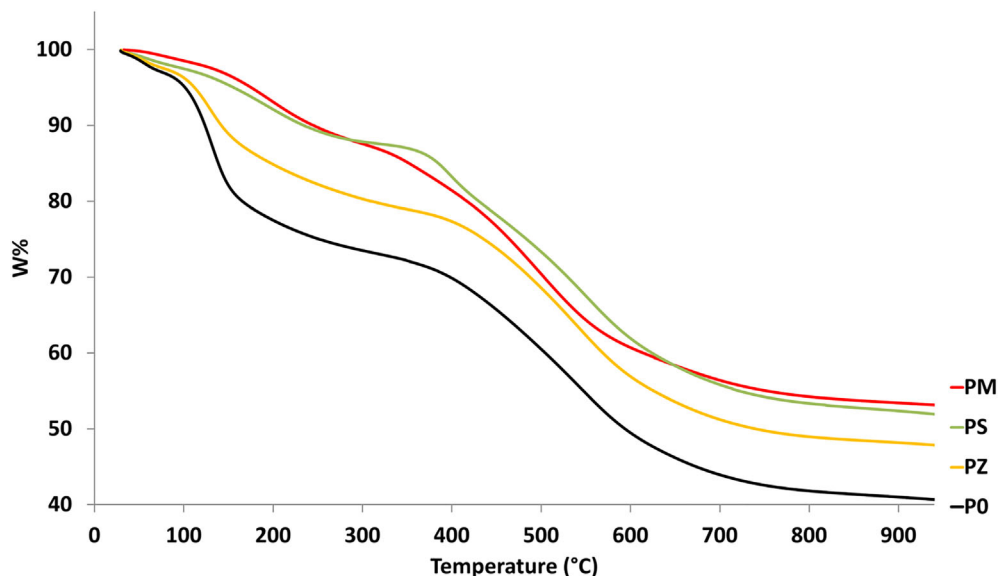
The thermogravimetric curves in Figure 8 show that the addition of nano-particles can change the final residual weight after the complete pyrolysis decomposition process. In particular at  $940^\circ C$ , temperature for which the



TABLE 6 Compressive tests results

	MP0	MPZ	MPS	MPM
Compressive modulus of elasticity (GPa)	48.56 ± 3.45	109.72 ± 11.73	102.73 ± 23.93	63.00 ± 8.12
Maximum stress (MPa)	0.770 ± 0.097	1.225 ± 0.231	1.428 ± 0.137	1.318 ± 0.193

FIGURE 8 TGA curves for samples P0, PZ, PM, PS



plateau is fully reached for each sample, the percentage residual weight of the sample P0 is 40.68%, while for nano-filled samples PZ, PM and PS it is respectively 47.87%, 53.14%, and 51.94%. SiC and MgO influence more deeply the behavior of the resin and, thanks to their addition, the char yield is higher. Obviously, the ceramic nano-particles are inherit at the TG test conditions and their proper weight is added to the residual char. Considering 5% wt with respect to the resin, the results still confirms that nano-particles can improve the final char yield. This result is coherent with the influence that the nano-particles can have in polymer properties: they can alter the crosslink density<sup>[27]</sup> which is strictly correlated with the char yield, and also the thermal stability.<sup>[28]</sup> In fact, near to nano-particles surface, there is an interphase zone where the polymer chains are entangled each other with adsorbed and unabsorbed segments: this zone have different properties compared with the net material and it can influence the thermal stability too.<sup>[8,29]</sup>

### 3.4 | FTIR studies

FT-IR spectroscopy is an extremely useful technique for the qualitative and semi-quantitative analysis of solid phase organic compounds such as phenolic resins. Figure 9 shows the spectrum of the bulk phenolic resin (P0), where the characteristic features of the phenolic resin can be identified. The broad peak at 3350  $\text{cm}^{-1}$  can be assigned to

the O—H bond stretching vibrations, the peaks at around 2900  $\text{cm}^{-1}$  are attributed to the C—H and methylene bridges stretching, the aromatic C=C stretching vibrations can be found at 1650  $\text{cm}^{-1}$ , at 1450 and 1233  $\text{cm}^{-1}$  the stretching vibrations relative to the CH<sub>2</sub>—O—CH<sub>2</sub> ether bridges, and lastly the 820 and 750  $\text{cm}^{-1}$  peaks can be assigned to aromatic C—H bending out-of-plane vibrations.<sup>[30,31]</sup> The latter group of peaks is of particular interest to the study of the aromatic rings substitution and thus the cross-linking degree. In fact, the peak at 820  $\text{cm}^{-1}$  can more precisely be attributed to the bending out of plane of an aromatic ring substituted at the positions 1 and 2, whereas the peak at 750  $\text{cm}^{-1}$  corresponds to the vibration of a ring substituted at positions 1, 2 and 3, that is a ring system with a single isolated C—H bond (Table 7).<sup>[31]</sup> Since the nanoparticles may affect the cure mechanism and this may lead to different cross-linking degrees, it is useful to compare the spectra of the nano-charged samples in this area of the IR spectrum (Figure 9).

As shown in Table 7, the intensity ratio corresponding to the peaks at 754 and 820  $\text{cm}^{-1}$  can be correlated to the presence of substituted aromatic rings. This value is higher for the phenolic resin charged with MgO (PM), whereas is lower for P0 and PZ, both showing a similar ratio. The data indicates a higher presence of di-substituted phenolic rings for PM, thus suggesting a higher cross-linking degree in presence of MgO nanoparticles.<sup>[31]</sup> This result can be explained considering the catalytic effect of the Mg<sup>2+</sup> O<sup>2-</sup> active sites, contained on the MgO

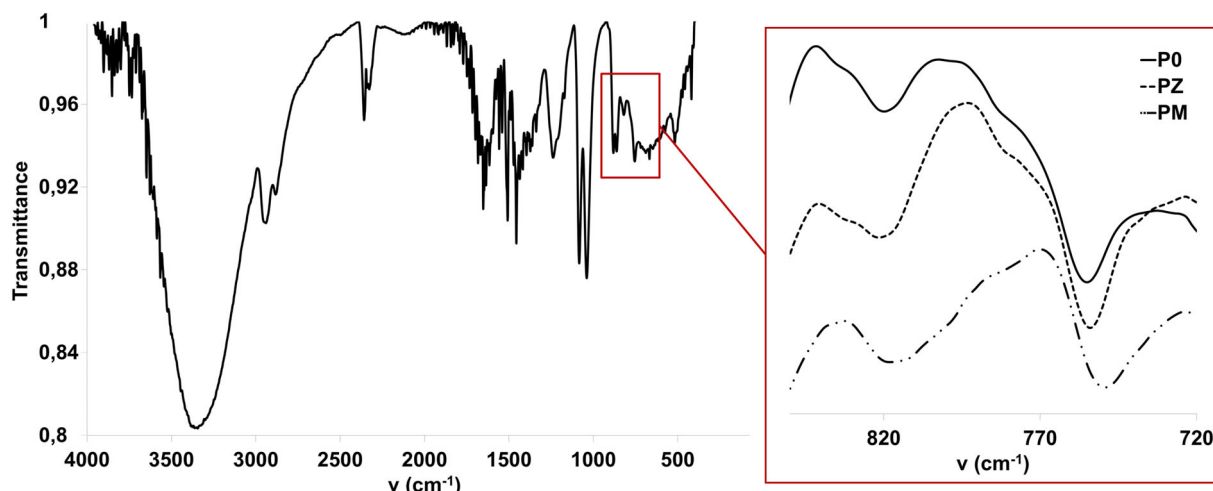
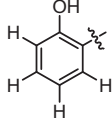
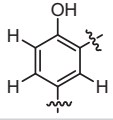


FIGURE 9 FTIR spectra of sample P0 compared with PZ and PM

TABLE 7 FTIR data of sample P0 compared with PZ and PM

Sample	Nano-particles (wt%)	$(1-T)_{754}/(1-T)_{820}$	Aromatic ring system	Peak frequency (cm <sup>-1</sup> )
P0	0	1.50 ± 0.06		760–750
PZ	5 (ZrO <sub>2</sub> )	1.40 ± 0.05		
PM	5(MgO)	1.08 ± 0.08		825–815

nanoparticle surface, a phenomenon previously reported in literature<sup>[32]</sup> that clarifies not only the higher cross-linking degree of PM, but also the shorter cure time recorded for this kind of nano-charged resin.

### 3.5 | Oxyacetylene flame exposure

The oxyacetylene flame exposure was carried out with a constant heat flux of 4 MW/m<sup>2</sup> for 90 s. The tip of the torch was positioned at the right distance from the sample surface for obtaining the desired incident heat flux. During the approach of the torch the samples are shielded with insulating panels, in order to avoid an undesired pre-heating. At the end of the exposure time, samples were quickly cooled down by a CO<sub>2</sub> gas stream in order to avoid post-test oxidation phenomena. For each kind of sample, three different specimens were tested and the reported data are the average value of three tests. Figure 10 shows some representative samples after the exposure test; at a first glance the color of the surfaces is different: MP0 has the typical dark gray of a carbonaceous residue and it is uniform on the whole

surface. The other samples, modified by nanoparticles, show the presence of a brighter surface residue after the flame exposure test. The inspection of the post-test samples surface highlights different morphologies for the different compositions: the surface of MP0 and MPZ is quite homogeneous and does not show the presence of surface cracks, while MPS and MPM samples present several surface cracks and, for MPM composition, also a partial spallation of the surface residue material. The surface recession was evaluated as the difference between the initial sample height (30 mm) and the minimum height after the test. The spot of the oxyacetylene flame was smaller than the exposed surface, thus the central part of the samples, that directly faces the torch, is subjected to a deeper recession: for this reason both the central and lateral recession are taken into account and are reassumed in Table 7. MP0 and MPM samples show a greater surface recession and also the maximum difference between the central and lateral recession; on the contrary ZrO<sub>2</sub> and SiC-modified samples exhibit the best performance in terms of central recession and also a smaller gap between the central and lateral surface recession data. The mass loss of the samples provides other important



FIGURE 10 Pictures of samples after the oxyacetylene flame exposure

TABLE 8 Percentage mass loss, central and lateral recession, maximum surface and back temperature and their difference for samples exposed to the oxyacetylene flame

Sample	Mass loss (%)	Central surface recession (%)	Lateral surface recession (%)	Maximum surface temperature (°C)	Maximum back temperature (°C)	$\Delta T_{90s}$ (°C)
MP0	23.12 ± 0.36	10.27 ± 0.38	6.42 ± 1.10	2183.63 ± 2.68	414.39 ± 21.12	1769
MPZ	21.46 ± 1.13	7.73 ± 1.82	5.41 ± 0.82	2023.75 ± 17.40	357.42 ± 20.91	1657
MPS	22.19 ± 0.35	7.22 ± 0.56	5.91 ± 0.24	2186.73 ± 12.92	373.98 ± 8.67	1813
MPM	27.67 ± 0.92	10.58 ± 1.96	6.87 ± 0.76	2145.91 ± 45.53	326.04 ± 37.05	1820

information about the goodness of the ablative materials: all the samples were manufactured with the same phenolic resin and carbon felt, thus the differences in the mass loss can be connected with the nano-fillers addition which can influence the mechanical properties of the char layer (hindering or promoting its removal), the thermal conductivity and also the pyrolysis processes.<sup>[8,28]</sup> Data about the mass loss are reported in Table 8: the addition of ZrO<sub>2</sub> and SiC nano-particles does not alter substantially the mass loss in comparison with plain samples, in particular considering the standard deviation. On the other hand, the addition of MgO nano-particles causes an increase in mass loss (5%) and, contextually, an almost negligible increment in the surface recession (only +1% if compared with MP0): the discrepancy between these two data can be induced by the detaching of MPM samples fragments, which strongly influences the weight loss but not necessarily the surface recession. Obviously a possible influence of the MgO on the pyrolysis phenomena is not excluded, but this hypothesis needs further investigations.

The trend of the surface and back temperatures recorded during the tests is shown in Figure 9 and the maximum temperature values are reported in Table 7. For MP0, MPS, and MPM samples the surface temperature trend is very similar: the temperature reaches very quickly the value of about 2100°C and then it slightly increases during the test. On the contrary the surface temperature of MPZ samples reaches its maximum value after few seconds of exposure and then it remains

quite constant during the test with a gradual decrease until the heat flux is removed. At the end of the exposure time of 90 s, the surface temperature of MP0 and MPS are similar and higher than the other two tested materials (Figure 11). After the oxyacetylene flame test the samples were cut along their main axis, polished and prepared in order to observe their cross section with a scanning electron microscope. In Figure 12 the SE micrographs of the exposed surface show the morphology of the pyrolyzed resin and enlighten only a slight difference in the roughness of the MPS sample. The BSE micrographs show the nano-particles distribution after the test: as already observed in other works<sup>[8,10,11,33,34]</sup> a phenomenon of partial melting and/or coalescence of the ceramic nano-particles is evident. ZrO<sub>2</sub> nano-particles seem to be partially molten, coalescing in sub-micrometer clusters. The outer surface of the MPS sample appears depleted of ceramic particles probably because of the formation of volatile products during the exposure to the oxyacetylene flame.<sup>[20]</sup> The observed areas, just below the exposed surface, are rich of spherical ceramic particles (Figure 10) which at the EDS analysis results to contain Si and O: according to the condition of temperature and pressure, the SiC nano-particles can react with the oxygen producing liquid SiO<sub>2</sub> (reaction 1) which forms spherical particles during the cooling, but for higher temperatures the reactions (2) and (3) are active and volatile SiO is produced.<sup>[20,21,33]</sup>



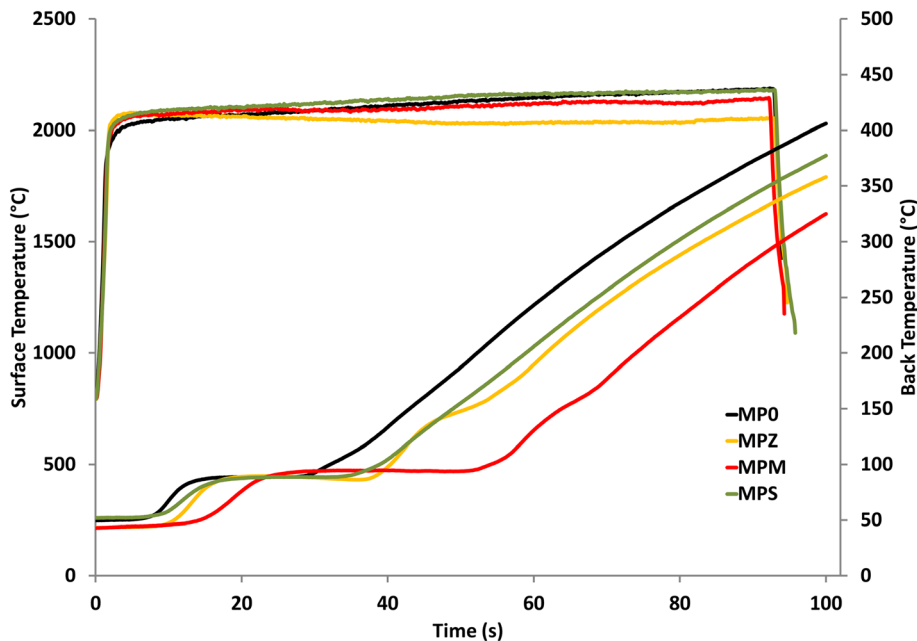


FIGURE 11 Surface and back temperature recorded during the oxyacetylene flame exposure (representative curves)

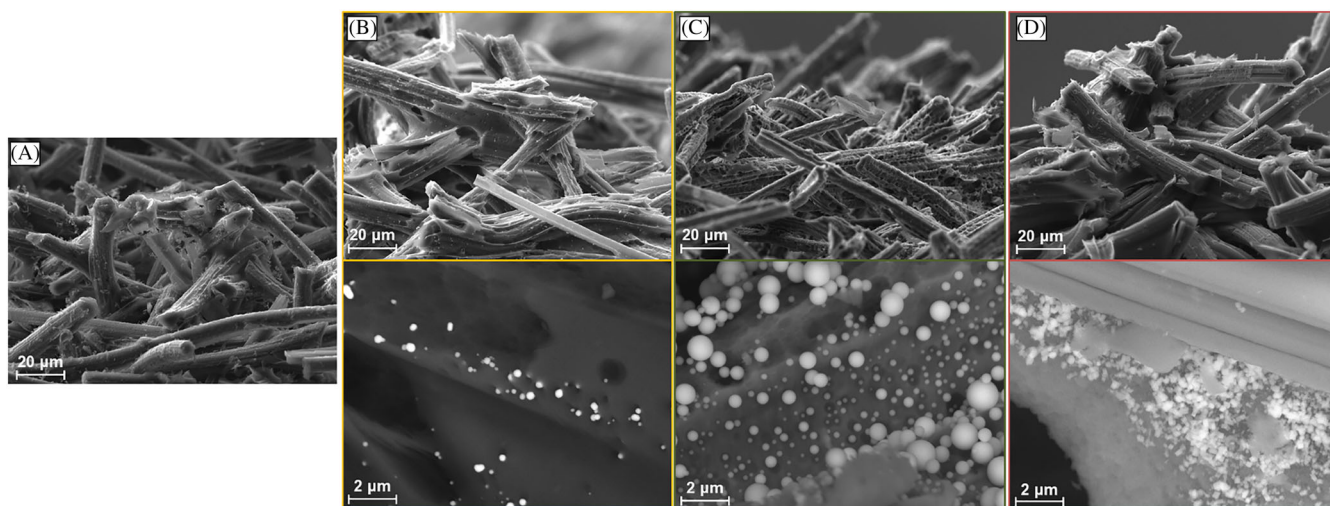
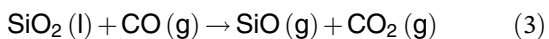
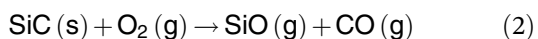


FIGURE 12 SE and BSE micrographs of the charred layer after the oxyacetylene flame exposure



The value of temperature for which the reactions (2) and (3) are active depends on the oxygen partial pressure and Ghelich et al.<sup>[20]</sup> proposed a threshold temperature of 2100°C that is coherent with the phenomena observed in MPS samples. In fact, on the exposed face, (maximum temperature higher than 2180°C) no SiC or SiO<sub>2</sub> particles were observed after the exposure test, but just below the surface the formation of spherical particles of SiO<sub>2</sub> is well evident (Figure 10).

Exploring all the cross section of the sample, it is possible to observe that in the bottom of the sample, the SiC nano-particles remain of the same dimension and morphology as in the virgin manufactured samples, but at about 3 mm from the exposed surface the morphology changes and EDS analysis reveals the presence of SiO<sub>2</sub> particles (according to quantitative elemental analysis) with an irregular shape and smaller diameters compared with the ones found close to the exposed surface (Figure 13).

The best results in terms of thermal protection was provided by the MPM samples. In addition, in this case the phenomenon of coalescence of the nano-particles was observed, as shown in Figure 10. The particles remain of

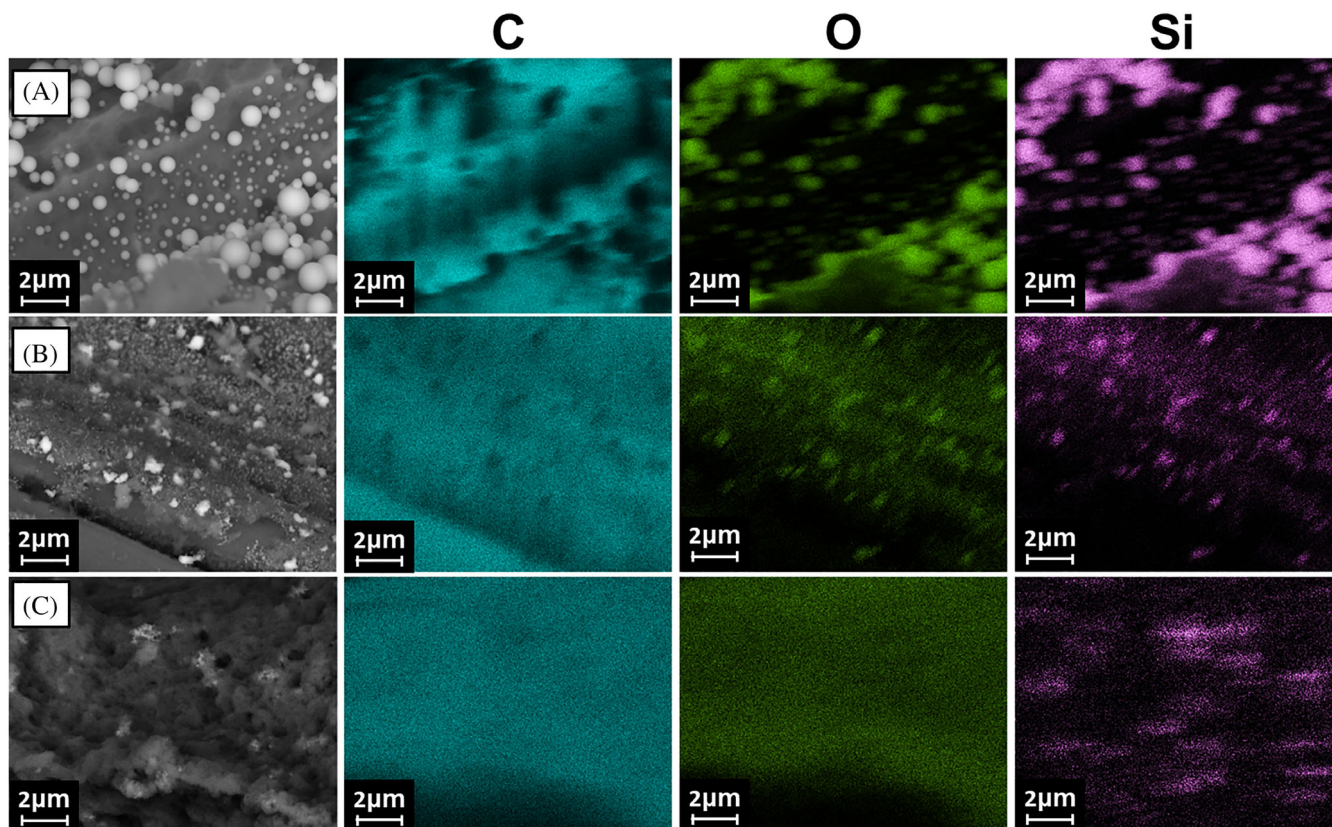


**FIGURE 13** EDS analysis for nano-particles of SiC in the charred sample MPS near the exposed surface (A), at about 2.5 mm from the exposed surface (B), and at the bottom (C)

small dimension, comparable or slightly larger than the initial ones, but they tend to form agglomerates in the pyrolyzed resin: moreover a phenomenon of shape modification was enlighten for the MgO nano-particles, both on the exposed face and within the sample for a thickness of about 5 mm from the outer surface. Figure 12 shows that the MgO nano-particles exhibit a change in the morphology induced by the high temperature exposure during the flame test, thus undergoing a shape modification from spherical to cubic. Moreover the particle size of dispersed cubic nano-MgO varies as a function of the distance from the exposed surface, thus showing a strong dependence from the thermal history experienced by the nano-particles during the test. Further XRD and SEM analyses were carried out on the MgO particles, both in the “as received” state and extracted from the char layer of the exposed samples, in order to better understand the mechanisms related to the particle size and shape modification observed in the exposed MPM samples. MgO particles were extracted from the tested samples by cutting the char layer and heating it at 800°C for 1 h in order to eliminate all the carbonaceous residue and the carbon fibers.

The results of the X-ray diffractions show that the as-received MgO powder reveals the presence of Mg(OH)<sub>2</sub> (brucite), while the particles extracted from char layer, only consist of periclase (MgO) phase which has the typical cubic morphology observed in the micrographs (Figure 14).<sup>[35]</sup> This variation in composition can be attributed to the high temperature exposure: the Mg(OH)<sub>2</sub> undergoes a reaction of dehydration producing MgO and H<sub>2</sub>O at temperature higher than 550°C at a pressure of 1 atm.<sup>[36]</sup> Another work<sup>[37]</sup> shows that for brucite nano-particles the dehydration reaction can occur at about 300°C, leading to formation of MgO nano-particles and the DSC analysis showed an exothermic peak corresponding to the dehydration reaction. Thus the presence of the Mg(OH)<sub>2</sub> in the nano-composite ablator is not to be considered beneficial because of the heating phenomena associated to the brucite transformation.

#### 4 | CONCLUSIONS

ZrO<sub>2</sub>, SiC and MgO nano-particles were selected as fillers for phenolic resin composites because of their high

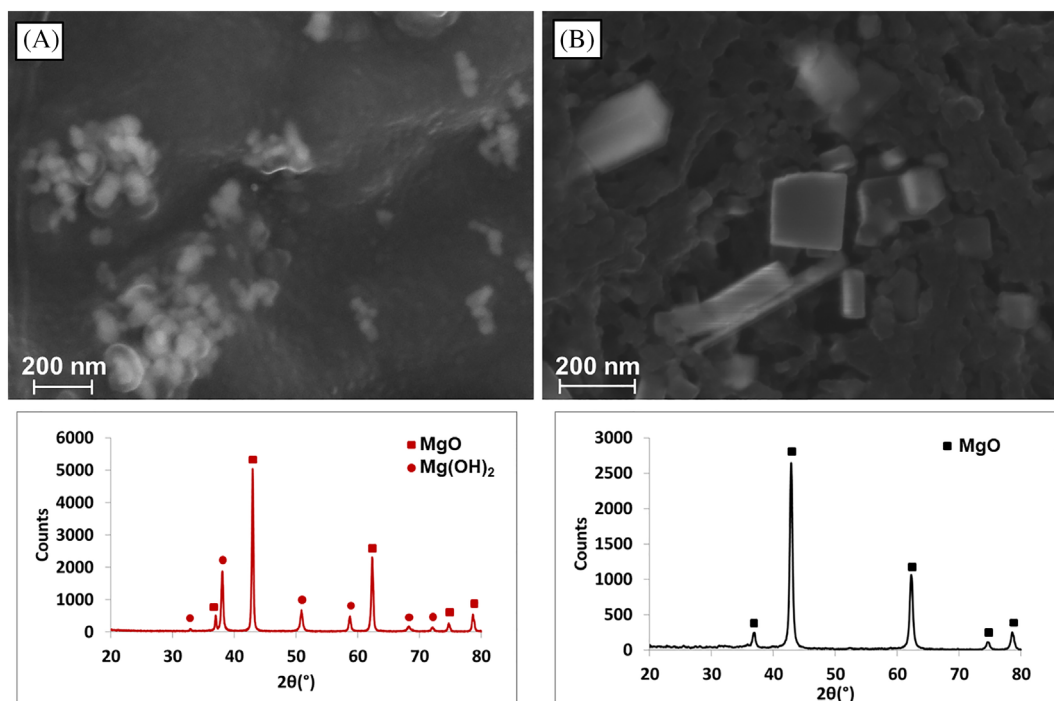


FIGURE 14 MgO particles before and after the oxyacetylene flame exposure (SE micrographs and XRD spectra)

melting point, low density and low thermal conductivity. In order to fully understand the effect of the nano-fillers, two kinds of nano-composite materials were manufactured: in a first step nano-particles were added to bulk phenolic resin (samples PZ, PS, PM) and then standard carbon-phenolic ablators were modified by the addition of ceramic nanoparticles (samples MPZ, MPS, MPM). The manufacturing strategies were optimized in order to guarantee a good dispersion and distribution of nano-particles and to confer the desired properties at the materials. The manufacturing procedures elaborated for the bulk samples are successful for  $ZrO_2$  and MgO, while in the PS samples SiC nano-particles are not satisfyingly distributed. The addition of MgO nano-particles to carbon-phenolic ablators leads to the reduction of gelation time of the resin-ethylene glycol solution. FTIR analysis revealed that MgO particles are able to promote the network formation during the polymerization of the phenolic resin: this is a very interesting property because the shorter the gelation time the lower the possibility of nano-particles agglomeration. As proved by compression tests on charred standard and nano-composites ablators, ceramic nano-particles are able to improve the mechanical performance of the char: this result is of interest since the external charred layer of an ablative shield need to withstand intense shear stress because of the friction with the atmosphere.

The oxyacetylene torch tests reveal a significant performance improvement when nano-particles are added to the standard material. Coalescence phenomena are

evident for  $ZrO_2$ -based ablators leading to the formation of a ceramic shell on the surface of the exposed samples. The test conditions on the exposed surface let SiC nano-particles form volatile products while just under the exposed face, SiC reacts with the available oxygen forming  $SiO_2$ , which solidifies in spherical particles at the end of the test.  $ZrO_2$  and MgO nano-particles form a layer on the surface of the exposed samples and, for this reason, there is a variation in the recorded surface temperature. On the contrary SiC volatilizes during the test and no variation of surface temperature was observed if compared to the standard ablator MP0. The back surface temperature is always lower for the ablators modified by nano-particles: MgO guarantees the greater drop in temperature between back and exposed surface, while  $ZrO_2$  guarantee the lower mass loss and surface recession. The results of this work show that nano- $ZrO_2$  and nano-MgO can be promising candidates as nano-fillers for carbon-phenolic ablators.

#### FUNDING INFORMATION

The authors did not receive support from any organization for the submitted work. Open access funding provided by Università degli Studi di Roma La Sapienza within the CRUI-CARE Agreement.

#### ACKNOWLEDGMENT

Open Access Funding provided by Università degli Studi di Roma La Sapienza within the CRUI-CARE Agreement.

## CONFLICT OF INTEREST

The authors declare that they have no conflict of interest.

## DATA AVAILABILITY STATEMENT

The datasets generated during and/or analyzed during the current study are available from the corresponding author on reasonable request.

## ORCID

Laura Paglia  <https://orcid.org/0000-0001-9112-2297>

## REFERENCES

- [1] F. Hussain, *J. Compos. Mater.* **2006**, *40*, 1511.
- [2] A. J. Crosby, J. Y. Lee, *Polym. Rev.* **2007**, *47*, 217.
- [3] E. Roduner, *Chem. Soc. Rev.* **2006**, *35*, 583.
- [4] D. Chakravorty, *Bull. Mater. Sci.* **1992**, *15*, 5.
- [5] K. Niihara, *J. Sci. Soc. Jpn.* **1991**, *99*, 974.
- [6] M. Natali, J. M. Kenny, L. Torre, *Prog. Mater. Sci.* **2016**, *84*, 192.
- [7] S. Fu, Z. Sun, P. Huang, Y. Li, N. Hu, *Nano Mater. Sci.* **2019**, *1*, 2.
- [8] L. Paglia, V. Genova, M. P. Bracciale, C. Bartuli, F. Marra, M. Natali, G. Pulci, *J. Therm. Anal. Calorim.* **2020**, *142*, 2149.
- [9] P. R. Matli, A. V. Krishnan, V. Manakari, G. Parande, B. W. Chua, S. Wong, C. Lim, M. Gupta, *Integr. Med. Res.* **2020**, *9*, 3664.
- [10] L. Paglia, V. Genova, F. Marra, M. P. Bracciale, C. Bartuli, T. Valente, G. Pulci, *Polym. Degrad. Stab.* **2019**, *169*, 108.
- [11] G. Pulci, L. Paglia, V. Genova, C. Bartuli, T. Valente, F. Marra, *Compos. Part A: Appl. Sci. Manuf.* **2018**, *109*, 330. <https://doi.org/10.1016/j.compositesa.2018.03.025>
- [12] W. Li, T. Wang, Z. Zhang, J. Zhang, Z. Dong, H. Huang, J. Liang, *Polym. Compos.* **2021**, *42*, 6749.
- [13] I. Srikanth, A. Daniel, S. Kumar, N. Padmavathi, V. Singh, P. Ghosal, A. Kumar, G. R. Devi, *Scr. Mater.* **2010**, *63*, 200.
- [14] T. Mary, M. S. Chandran, S. Jishnu, K. Sunitha, R. S. Rajeev, D. Mathew, N. Sreenivas, L. A. Pillai, C. Nair, *Polym. Adv. Technol.* **2015**, *26*, 104.
- [15] J. M. Park, D. J. Kwon, Z. J. Wang, J. U. Roh, W. I. Lee, J. K. Park, K. L. Dvreis, *Compos. B: Eng.* **2014**, *2014*(67), 22.
- [16] B. Bakhshi, M. Heydarian, *Polym. Compos.* **2021**, *42*, 3892.
- [17] R. B. Mathur, B. P. Singh, T. L. Dhama, Y. Kalra, N. Lal, R. Rao, A. M. Rao, *Polym. Compos.* **2010**, *31*, 321.
- [18] K. Rocznik, M. Skarzynski, *J. Appl. Polym. Sci.* **1983**, *28*, 531.
- [19] G. Pulci, J. Tirillò, F. Marra, F. Fossati, C. Bartuli, T. Valente, *Compos. Part A: Appl. Sci. Manuf.* **2010**, *41*, 1483.
- [20] R. Ghelich, R. M. Aghdam, R. Z. Jahannama, *J. Compos. Mater.* **2018**, *52*, 1239.
- [21] S. Wang, H. Huang, Y. Tian, J. Huang, *Ceram. Int.* **2020**, *46*, 16151.
- [22] ASTM International D7264/D726M-15, *Standard Test Method for Flexural Properties of Polymer Matrix Composite Materials* **2010**.
- [23] ASTM C165-07, *Standard Test Method for Measuring Compressive Properties of Thermal Insulations* **2012**.
- [24] ASTM International E285-08, *Standard Test Method for Oxyacetylene Ablation Testing of Thermal Insulation Materials* **2020**.
- [25] Y. Ma, Y. Yang, C. Lu, D. Xiao, S. Wu, Y. Liu, *Polym. Compos.* **2018**, *39*, 1928.
- [26] F. Marra, G. Pulci, J. Tirillo, C. Bartuli, T. Valente, *Proc. Inst. Mech. Eng. Part. L J. Mater. Des. Appl.* **2011**, *225*, 32.
- [27] P. Dittanet, R. A. Pearson, P. Kongkachuichayc, *Int. J. Adhes. Adhes.* **2017**, *78*, 74.
- [28] M. Rallini, L. Torre, J. M. Kenny, M. Natali, *Polym. Compos.* **2017**, *38*, 1819.
- [29] D. Ciprari, K. Jacob, R. Tannenbaum, *Macromolecules* **2006**, *39*, 6565.
- [30] H. Cheng, C. Hong, X. Zhang, H. Xue, S. Meng, J. Han, *Nat. Publ. Gr.* **2016**, *1*, 9.
- [31] J. I. Di Cosimo, V. K. Diez, C. Ferretti, C. R. Apesteguía, *Catalysis* **2014**, *26*, 1.
- [32] Y. Y. Zhang, Y. F. Zhang, L. J. He, Z. F. Zhou, *J. Adhes. Sci. Technol.* **2007**, *21*, 833.
- [33] A. Mirzapour, M. H. Asadollahi, S. Baghshaei, M. Akbari, *Compos. Part A: Appl. Sci. Manuf.* **2014**, *63*, 159.
- [34] L. Paglia, V. Genova, J. Tirillò, C. Bartuli, A. Simone, G. Pulci, F. Marra, *Appl. Compos. Mater.* **2021**, *28*, 1675.
- [35] C. Liu, D. Wang, H. Zheng, T. Liu, *Phys. Chem. Miner.* **2017**, *44*, 297.
- [36] X. Zheng, B. Cordonnier, W. Zhu, F. Renard, B. Jamtveit, *Geochim. Geophys. Geosys.* **2018**, *19*, 2661.
- [37] R. Wahab, S. G. Ansari, M. A. Dar, Y. S. Kim, H. S. Shin, *Mater. Sci. Forum* **2007**, *558-559*, 983. <https://doi.org/10.4028/www.scientific.net/MSF.558-559.983>

**How to cite this article:** L. Paglia, C. Mapelli, V. Genova, M. P. Bracciale, F. Marra, C. Bartuli, I. Fratoddi, G. Pulci, *Polym. Compos.* **2022**, *1*. <https://doi.org/10.1002/pc.26811>